Original Article

Diane-35 and metformin therapy in rats with endometrial lesions induced by dihydrotestosterone exposure

Yanjun Liu[1,2,3], Ran Xu[4], Yifan Zhou[1,2,3], Yang Wang[2,3], Feifei Zhang[2,3], Xiaoyu Tong[5], Peng Cui[6], Tong Ma[5], Jian Sun[7], Yi Feng[5], Xin Li[2,3]

[1]Department of Obstetrics and Gynecology, Shanghai Medical School, Fudan University, Shanghai, China; [2]Shanghai Key Laboratory of Female Reproductive Endocrine Related Diseases, Fudan University, Shanghai, China; [3]Department of Gynecology, Obstetrics and Gynecology Hospital of Fudan University, Shanghai, China; [4]Department of Cardiovascular Surgery, Shanghai Chest Hospital, Shanghai Jiao Tong University, Shanghai, China; [5]Department of Integrative Medicine and Neurobiology, School of Basic Medical Sciences, Institutes of Brain Science, Brain Science Collaborative Innovation Center, State Key Laboratory of Medical Neurobiology, Institute of Acupuncture and Moxibustion, Fudan Institutes of Integrative Medicine, Fudan University, Shanghai, China; [6]Department of Anesthesiology, Yueyang Hospital of Integrated Traditional Chinese and Western Medicine, Shanghai University of Traditional Chinese Medicine, Shanghai, China; [7]Department of Breast Surgery, Obstetrics and Gynecology Hospital of Fudan University, Shanghai, China

Contributions: (I) Conception and design: Y Liu, X Li, Y Feng; (II) Administrative support: R Xu, Y Liu, Y Zhou, Y Wang, F Zhang; (III) Provision of study materials or patients: X Li; (IV) Collection and assembly of data: Y Liu, R Xu, X Li, Y Feng, J Sun, X Tong, P Cui, T Ma; (V) Data analysis and interpretation: Y Liu, R Xu; (VI) Manuscript writing: All authors; (VII) Final approval of manuscript: All authors.

Correspondence to: Yi Feng. State Key Laboratory of Medical Neurobiology, Institute of Acupuncture and Moxibustion, Fudan Institutes of Integrative Medicine, Fudan University, No. 138, Medical College Road, Xuhui District, Shanghai 200032, China. Email: fengyi17@fudan.edu.cn; Xin Li. Department of Gynecology, Obstetrics and Gynecology Hospital of Fudan University, No. 419, Fangxie Road, Huangpu District, Shanghai 200032, China. Email: lxsure1501@163.com.

Background: Cotreatment with metformin and Diane-35 is conventionally used in the clinic to ameliorate ovulatory dysfunction and insulin resistance in women with polycystic ovary syndrome (PCOS). We previously showed that this combination treatment could reverse endometrial hyperplasia and endometrial cancer (EC) in patients with PCOS. Here, we aimed to investigate the influence of dihydrotestosterone (DHT) and this cotreatment on the endometrium, along with the related mechanisms.

Methods: We treated a DHT-exposed rat model with Diane-35 or metformin alone or their combination and investigated the 3-dimensional (3D) endometrial structure to determine the role of these treatments in reversing endometrial lesions and to clarify the underlying mechanisms. Uterine segments were made transparent with clear, unobstructed brain/body imaging cocktails and a computational analysis protocol and then labeled with 4',6-diamidino-2-phenylindole (DAPI), antiandrogen receptor (AR) antibody, and antiglucose transportation protein 4 (GLUT4) antibody. We visualized and analyzed the endometrial structure, AR expression, and GLUT4 expression under 3D conditions using light sheet microscopy and Imaris software (Bitplane, Zurich, Switzerland).

Results: Long-term DHT treatment contributed to hyperandrogenism and insulin resistance in female Wistar rats. After DHT treatment, rats exhibited other PCOS-like characteristics, such as polycystic ovary morphology, hypothalamic-pituitary-ovarian axis disorder, and relative endometrial hyperplasia. After metformin and Diane-35 treatment, the PCOS-like characteristics and endometrial hyperplasia were alleviated.

Conclusions: Hyperandrogenism and insulin resistance likely play important roles in the pathophysiological changes of PCOS and lead to PCOS-like characteristics as well as endometrial lesions. Hypoandrogenic and insulin sensitization therapy can alleviate DHT-induced endometrial hyperplasia by regulating AR and GLUT4 expression.

Keywords: Diane-35; metformin; polycystic ovary syndrome (PCOS); endometrium; CUBIC 3-dimensional tissue clearing

Submitted Aug 17, 2021. Accepted for publication Oct 09, 2022. Published online Feb 02, 2023.
doi: 10.21037/atm-21-2441
View this article at: https://dx.doi.org/10.21037/atm-21-2441

Introduction

Polycystic ovary syndrome (PCOS) is characterized by excessive androgen production, ovulatory dysfunctions, polycystic ovary morphology, and obvious metabolic disorders, such as insulin resistance and compensatory hyperinsulinemia. PCOS has an incidence of approximately 4–21% in different regions and populations of different races, and its incidence in China is 5.6% (1,2). Patients with PCOS have a significantly increased risk of developing endometrial cancer (EC). The morbidity of EC among patients with PCOS is 9%, which is 3 times higher than that among healthy women (3-5).

EC is one of the most common gynecological malignant tumors worldwide, and its incidence is increasing (6). Traditional treatments for EC include hysterectomy, bilateral adnexectomy, platinum- and paclitaxel-based chemotherapy, and pelvic or vaginal brachytherapy. Because uterine bleeding occurs early in EC, it is often diagnosed at an early stage, making conservative treatment possible. Conservative treatment offers new hope for 14% of premenopausal patients and 5% of EC patients under 40 years of age who wish to preserve their fertility while receiving antitumor therapy (7).

In 2014, the National Comprehensive Cancer Network (NCCN) recommended medroxyprogesterone acetate (MPA) as a conservative treatment option for EC. In the same year, Li *et al.* (8) reported that metformin combined with Diane-35 had a 90% reversal rate in patients with early EC. This rate was significantly higher than the 66% remission rate of MPA reported by Zhao *et al.* (9). A large number of studies on EC have shown that progesterone-based therapies can result in a 30% rate of EC chemoresistance after long-term treatment (10).

Metformin, a synthetic derivative of guanidine, has been used clinically in the treatment of diabetes for more than 50 years (11). The effect of metformin on insulin sensitization and the improvement of insulin resistance is mainly attributed to its ability to regulate energy metabolism. Diane-35, composed of 2 mg of cyproterone acetate and 35 μg of ethinylestradiol, is an oral contraceptive agent (12,13). In addition to the strong antiandrogenic effect of Diane-35 (14), its estrogen component can increase the sensitivity of the progesterone receptor (PGR) (15), while its progesterone component can effectively antagonize endometrial hyperplasia and carcinogenesis (6,16). The effect of metformin combined with Diane-35 on EC has been confirmed in many studies. The two components of Diane-35 have converse effects on the endometrium: the estrogen component prompts endometrium proliferation, while the concomitant administration of progestin with the estrogen leads to the downregulation of estrogen receptors and increased metabolic inactivation, which is associated with a lower proliferation rate of the endometrium (17). The antitumor mechanism of metformin mainly operates via its ability to promote the expression of PGR and other antitumor biomarkers, a phenomenon which has been observed in EC cell lines and in patients with EC (18).

This study aimed to investigate the impact of hyperandrogenism and insulin resistance on the endometrium and the mechanism by which the combined treatment cures PCOS-related endometrial hyperplasia. We used high-concentration, long-term dihydrotestosterone (DHT) treatment to establish hyperandrogenism and

Highlight box

Key findings

- Hyperandrogenism and insulin resistance lead to PCOS-related endometrial lesions.
- Hypoandrogenic and insulin sensitization therapy can alleviate DHT-induced endometrial lesions by regulating AR and GLUT4 expression in rats.

What is known and what is new?

- Hypoandrogenic and insulin sensitization therapy have been used in clinic to alleviate the symptom of PCOS; however, their potential in treating endometrial lesions is unknown. The role and mechanism of hypoandrogenic and insulin sensitization therapy in DHT-induced endometrial lesions were investigated in our research, which, for the first time, used a 3-dimensional tissue clearing and imaging technique to measure endometrial lesions in rats.

What is the implication, and what should change now?

- Although our study revealed the role of AR and GLUT4 in DHT-induced endometrial lesions in rats, further experiments should be performed to identify them as potential targets to treat PCOS-related endometrial lesions *in vitro* or in human samples.

insulin resistance in Wistar rats and administered a 4-week treatment. Since methods for studying the pathophysiological changes in endometrial tissues are limited due to their thin and fragile texture and due to the very small sample size of these patients, we used an innovative 3-dimensional (3D) imaging method to investigate endometrial tissue. To the best of our knowledge, this is the first study to observe the rat uterus under 3D conditions by clear, unobstructed brain/body imaging cocktails and computational analysis (CUBIC). We present the following article in accordance with the ARRIVE reporting checklist (available at https://atm.amegroups.com/article/view/10.21037/atm-21-2441/rc).

Methods

Animals and treatments

Female Wistar rats [21 days old; weighing 49.43±1.73 g (mean ± SD)]; Shanghai SLAC Laboratory Animal Co. Ltd., Shanghai, China) were randomly divided into 5 groups (control, DHT, DHT + Diane-35, DHT + metformin, and DHT + Diane-35 + metformin) according to a random number table that was generated using the standard "= RAND ()" function in Microsoft Excel (Microsoft Corp., Redmond, WA, USA). These rats were allowed to acclimate for 3 days. The rats were housed at a density of 6 rats per experimental unit in cages under controlled conditions (21–22 ℃; 55–65% humidity; 12-h light-dark cycle; lights on at 7 a.m.; standard laboratory chow and water provided ad libitum). All experimental procedures performed on rats were conducted in compliance with the Management Rule of Laboratory Animals (Chinese Order No. 676 of the State Council, revised March 1, 2017). A protocol was prepared before the study without registration. This study was approved by the Animal Ethics Committee, School of Basic Medical Sciences of Fudan University, China.

DHT (7.5 mg) or empty tubes with or without DHT (Sigma, A8380) were generated with Silastic Laboratory Tubing (length, 1 cm; inner diameter, 1.5 mm; outer diameter 2.0 mm, GY-96115-10, Dow Corning, Midland, MI, USA) and Silastic Medical Adhesive Silicone (Type A, Dow Corning) (19-21). Diane-35 tablets (Bayer Schering Pharma AG, Leverkusen, Germany) containing 2.0 mg of cyproterone acetate and 35 of μg ethinylestradiol and Glucophage tablets (Sino-American Shanghai Squibb Pharmaceuticals Ltd., Shanghai, China) containing 500 mg of metformin were dissolved in 1% sodium carboxymethyl cellulose solution (CMC-Na) (9004-32-4, Sigma-Aldrich, St. Louis, MO, USA) to concentrations of 0.2035 and 10 mg/mL, respectively. The doses were translated from humans to rats based on the body surface area conversion formula (20,21).

The control rats were implanted with empty subcutaneous silicone tubes at 21 days of age and were gavaged with 1% CMC-Na at 60 days of age. The DHT group was implanted with a 7.5-mg DHT 90-day continuous-release tube on day 0. The DHT group was divided into the DHT (0.2 mL of 1% CMC-Na solution), DHT + Diane-35 (0.2 mL of 1% CMC-Na and 0.2035 mg/mL of Diane-35 solution), DHT + metformin (0.2 mL of 1% CMC-Na and 10 mg/mL of metformin solution), and DHT + Diane-35 + metformin (0.2 mL of 1% CMC-Na, 0.2035 mg/mL of Diane-35, and 10 mg/mL of metformin solution) groups. Each group was administered its respective treatment 49 days after DHT tube implantation. All tubes were subcutaneously transplanted in the posterior neck after isoflurane anesthesia. All tube transplantation and gavage administration procedures were performed by the same investigator. The treatment time was between 11.30 a.m. and 12.30 p.m. The investigation order was randomized daily, with each animal tested at a different time each test day.

In total, 33 rats were considered for the study, but 3 rats did not meet the inclusion criteria established before the experiment because their tube came off or because of a wound infection, and they were subsequently euthanized. Therefore, 30 rats (6 rats per group) that exhibited DHT-induced PCOS-like phenotypes, including a disordered estrous cycle, increased weight, and impaired glucose tolerance which indicated hyperandrogenism and insulin resistance, were ultimately included in the study (Figure S1). The sample sizes were estimated based on previous experience and previous studies (21). We selected a small sample size because the DHT-induced endometrial lesions were evaluated by the 3D imaging method for the first time in the present study, and the initial intention was to gather basic evidence regarding the use of this innovative method in more complex experimental designs. For each group, 3 different investigators were involved as follows: the first investigator (Y.L.) performed interventions, including tubing transplantation and gavage based on the randomization table and rat ear tags; the second investigator (R.X.) prepared these tubes and solutions for treatment and labeled these tubes and gavage syringes for each animal following the randomization table; and the third investigator (X.T.) prepared the randomization table, labeled all rats with ear tags, and grouped the rats into

the treatment groups for analysis. Due to obvious DHT-induced weight change, the experimenters could not be blinded to DHT or empty tube transplantation. Therefore, in order to avoid bias, all specimens, including blood, ovary, uterus, and vaginal smears, were relabeled again by the second investigator (R.X.) before analysis according to another new randomization table corresponding to the original table.

Growth curves of rats

Body weights were measured from day 0 before DHT tube transplantation to day 84 before the animals were euthanized (22). During the process, the food intake per cage (6 rats per cage) was recorded continuously every week and was calculated as the average food intake per rat per day. All the weight measurements were performed by the same investigator.

Estrous cycle determination

Vaginal smears were collected daily between approximately 11.30 a.m. and 12.30 p.m. from the 28th to the 37th day and on the 56th to the 80th day after the transplantation of DHT tubing. The investigation order was randomized daily, with each animal tested at a different time each test day. Plastic pipettes were filled with 10 mL of double-distilled water at ambient temperature and slowly inserted into the vaginas of restrained rats. After releasing the liquid, the tip was gently turned and rolled against the vaginal wall, and the liquid containing cells was collected and removed. Then, the cells were smeared onto a glass slide and air-dried naturally. Following Shorr's staining procedure, the stage of the estrous cycle was determined by microscopic analysis of the predominant cell type (Figure S2). In addition, the estrous cycle was reassessed by observation of the vaginal opening and cervical mucus crystallization (23-25). All vaginal smear analyses, image acquisitions, and image analyses were performed by the same investigator (Y.L.).

Oral glucose tolerance test (*OGTT*)

The OGTT was performed after the last treatment. After an overnight (12–14 h) fast, a blood sample was collected from a cut at the tip of the rat tail to determine the fasting blood glucose (FBG) level at 0 min. Then, 50% D-glucose solution was administered orally at a dose of 2 g/kg body weight via a blunt gavage needle (26,27). Blood samples were collected at 30, 60, and 120 min. Blood glucose concentrations were determined at 0, 30, 60, 120, and 180 min using a glucometer (Accu-Chek Performa, Roche Pharma, Basel, Switzerland) with its corresponding strips as soon as these samples were collected. All OGTT steps were performed by the same investigator (Y.L.), and the measurements were repeated twice to obtain the average.

Blood and tissue specimens

After the OGTT, all rats in the diestrus stage of the estrous cycle were fasted for 12–14 h and then underwent deep anesthesia. Blood samples were taken from the abdominal aorta, incubated in a refrigerator at 4 ℃ overnight, and then removed and centrifuged at 3,500 ×g for 15 min at 4 ℃. The upper serum was collected and stored in a −80 ℃ freezer with identifiable labels. Then, every rat was perfused with approximately 100 mL of phosphate-buffered saline (PBS; pH 7.4; 4 ℃; 10 mL/min) containing 10 U/mL of heparin until the outflow solution became colorless, which was followed by perfusion of approximately 100 mL of 4% (wt/vol) paraformaldehyde (PFA; pH 7.4; 4 ℃; 10 mL/min) until muscle stiffness occurred. The uteri and ovaries were carefully dissected, photographed, weighed, immersed in 4% PFA, and incubated at 4 ℃ for 24 h (28-30).

Hormone profile and biochemical indexes

An enzyme-linked immunosorbent assay (ELISA) kit (Sino-UK Institute of Biological Technology, Beijing, China) with a STAT FAX 2100 Microplate Reader (Awareness Technology Inc., Palm City, FL, USA) was used for measurements of estradiol (E2), free testosterone (FT), sex hormone-binding globulin (SHBG), luteinizing hormone (LH), follicle-stimulating hormone (FSH), prolactin (PRL), and serum fasting insulin (FINS) concentrations. All indices were tested during the diestrus stage after 12–14 h of fasting (21).

Homeostatic model assessment (HOMA)

The insulin resistance (HOMA-IR), insulin sensitivity (HOMA-IS), and β-cell function (HOMA-β) indices were calculated as follows: HOMA-IR index = FBG (mmol/L × FINS (mU/mL)/22.5; HOMA-IS index = 1/HOMA-IR; and HOMA-β index = 20 × FINS (m/mL)/[FBG (mmol/L) − 3.5] (%) (30).

Morphological analysis

At 1 day postfixation with 4% PFA, ovarian specimens were dehydrated in gradient ethanol, cleared in xylene, and embedded in paraffin. The embedded tissues were sliced into 5 mm-thick sections, and these were mounted on glass slides (31). The paraffin sections were stained with hematoxylin and eosin (HE) and observed by histomorphological examination under a light microscope (CM1850, Leica, Wetzlar, Germany). The number of cystic follicles and corpora lutea was counted. All results were confirmed by a pathologist.

Three-dimensional imaging with immunolabeling and data analysis

Because of the very small rat endometrium sample size and the fragile texture of this tissue, it was difficult to collect entire endometrial tissues and purify proteins or nucleic acids. Moreover, when the 2D imaging method is used, the diversity of different uterine segments can significantly bias the localization and quantification of key molecules. We performed the CUBIC clearing method according to the procedure described by Susaki *et al.* (32) and the immunostaining process according to the procedure described by Renier *et al.* (33), and the protocol was improved for uteri as described in Figure S3.

After 24 h of PFA fixation, the uterine tissues were washed with 10 mL of PBS for 6 h to remove the remaining PFA. The PBS solution was refreshed every 2 h. Then, PBS-washed uteri were moved to 5 mL of 1/2-water-diluted Reagent-1 and incubated for 6 h followed by the addition of 5 mL of Reagent-1 after discarding of the 1/2-water-diluted Reagent-1. Reagent-1 was used to remove lipids from inside the tissues, while 1/2-water-diluted Reagent-1 was used to form a concentration gradient that facilitated solution penetration. The whole process of lipid removal from the uterine tissue took 6 days, and Reagent-1 was replaced every 2 days. The tissue became relatively transparent after lipid removal.

To stop the clearing procedure and pretreat these samples before immunolabeling, we incubated the samples with 10 mL of PBS/0.2% Triton X-100 overnight. Subsequently, we blocked these samples in PBS/0.2% Triton X-100/6% goat serum for 2 h. Then, the samples were washed in PBS/0.2% Tween-20 (PBST) for 2 h and again for another 2 h after fresh PBST was added. After the removal of the clearing reagent, the samples returned to an opaque state, and after permeabilization and blocking, the samples were prepared for immunolabeling.

These samples were then incubated with primary antibodies (antibody against AR, cat. #ab74272, Abcam, Cambridge UK; antibody against GLUT4, cat. #ab35826, Abcam) diluted in PBST/6% goat serum for 2 days. The samples were then washed in PBST for 1 day, during which time fresh PBST was added 3 times, and the samples were then incubated with secondary antibodies (goat antimouse, cat. #A-11005, Invitrogen, Thermo Fisher Scientific, Waltham, MA, USA; goat antirabbit, cat. #A-11012, Invitrogen) and DAPI (D9542, Sigma-Aldrich) diluted in PBST/6% goat serum for another 2 days (Table S1). The samples were finally washed in PBST for 1 day, during which time fresh PBST was added 3 times, before refractive index (RI) matching was performed.

After immunofluorescence staining, 1/2-PBS-diluted Reagent-1 was added and incubated overnight or until the samples sank to the bottom. Then, the samples were transferred to Reagent-2 and incubated for at least 2 days until these samples achieved complete RI matching and became relatively transparent.

All these procedures were performed at 37 ℃ accompanied by gentle shaking at 60 rpm. To achieve good transparency, the incubation time was optimized according to the invidual characteristics of the uteri (such as thickness). For good immunolabeling quality, the antibody category and concentration were improved in preliminary experiments (Figure S4).

Three-dimensional images were collected using light sheet fluorescence microscopy (Light Sheet Z.1, Zeiss, Oberkochen, Germany). For each imaging experiment, the specimen was attached to the bracket with glue, and a 5× objective was used at a working distance of 3 mm. After scanning, the data were saved in CZI format and exported to IMS format using the Imaris File Converter v. 9.3.1 (Bitplane, Zurich, Switzerland). Images with multiple views were reconstructed by ImarisStitcher v. 9.2.0 (Bitplane) and analyzed using Imaris v. 9.5.0 (Bitplane). The surface algorithm of Imaris could semimanually identify the location and occupied space of the endometrium, myometrium, uterine glands, and fluorescent signal spots while quantifying the volume and signal intensity (Videos S1,S2,S3). For example, DAPI was used to label the cell nucleus. Due to the special structural characteristics of uterine tissue, glandular epithelial tissues could be outlined after staining with DAPI, as shown in Video S2. The surface mode of Imaris was used to identify and

calculate the volume of this gland automatically. All image acquisition and analysis processes were performed by the same investigator (Y.L.).

Statistical analysis

GraphPad Prism v. 7.0 (GraphPad Software, San Diego, CA, USA) and SPSS 23.0 (IBM SPSS Statistics, Armonk, NY, USA) were used for statistical analysis. No data were excluded from the data analysis. The distribution of variables was examined with the Shapiro-Wilk test, and the equality of variances was further tested using Levene test. Unless otherwise stated, an unpaired 2-tailed Student' *t*-test was used to analyze differences between all pairs of groups in parametric tests. One-way analysis of variance (ANOVA) followed by Tukey post hoc test and the Kruskal-Wallis 1-way ANOVA were used to evaluate the statistical significance among 3 or more groups for parametric and nonparametric tests (Table S2). The data are shown as the mean with SD or as the median with interquartile ranges. P values less than 0.05 were considered significant. No statistical method was used to predetermine the sample size. The sample sizes were estimated based on previous experience and previous studies. The study and experiments were both randomized and double-blinded.

Results

Excessive androgen production during prepuberty caused reproductive and metabolic disorders in female rats

To investigate the effect of continual DHT treatment on the PCOS phenotype in rats, we implanted DHT tubes in the rats in the DHT group (Figure S1). After implantation, the rats developed obvious PCOS-like features (*Figures 1-4*). Compared with those in the control group, the proportions of rats in the diestrus phase in the DHT-treated groups were significantly increased. The control group showed a regular 4- or 5-day 4-phase cycle, while the DHT groups showed disrupted estrous cycles, which remained mostly at the diestrus or metestrus phases (*Figure 1A*,*1B*). Two weeks after DHT implantation, the body weights of the rats in the DHT groups surpassed those of the rats in the control group, and the gap between the control and DHT treatment groups gradually increased over time (*Figure 2A*). In contrast to the rats in the control group, the rats in the DHT group had insulin resistance, as evidenced by the OGTT data (*Figure 2B*), the FINS concentration (*Figure 3G*), and HOMA scores (*Figure 3H*) in each group. Although the E2, FT, LH, and FSH levels were elevated (*Figure 3A*,*3B*,*3D*,*3E*), no differences in the SHBG or PRL concentrations were observed in those rats exposed to the continuous quantitative release of DHT (*Figures 3C*,*3F*). There were obvious differences in uterine and ovarian morphology between the control group and the DHT group. Continual DHT treatment led to smaller and slighter uteri and ovaries (*Figures 4A*,*4C-4E*). Ovaries from rats without DHT treatment consisted of follicles at different stages of development and exhibited normal numbers of corpora lutea. However, ovaries from rats administered DHT showed increased numbers of cystic follicles and fewer corpora lutea (*Figure 4B*).

Diane-35 and metformin mediated reversal of the PCOS phenotype

To further determine the role of Diane-35, metformin, and Diane-35 plus metformin treatment in the pathogenesis of the PCOS phenotype, these drugs were administered to rats with the DHT-induced PCOS-like phenotype by oral gavage, and 1% CMC-Na was administered to the rats in the DHT and control groups as the solvent control (Figure S1). Next, we measured the effects of Diane-35 and metformin on rats with the DHT-induced PCOS-like phenotype (*Figures 1-4*). After the beginning of treatment, the estrous cycles of the DHT-treated rats were gradually restored. Compared with the DHT + metformin group, which had a slow estrous cycle restoration time of 2 weeks of therapy, the DHT + Diane-35 and DHT + Diane-35 + metformin combination treatment groups had quicker 5-day reversal times (*Figure 1C-1E*). In addition, the administration of Diane-35 and metformin led to weight loss beginning in the first week of treatment. The Diane-35 group and Diane-35 + metformin group showed similar trends, while the metformin group demonstrated a more moderate decline (*Figure 2A*). In addition, the DHT-induced insulin resistance, abnormal hormone profiles, and aberrant ovarian morphology were ameliorated. While metformin obviously improved the OGTT performance (*Figure 2B*) and increased the SHBG levels (*Figure 3C*), Diane-35 had significant effects on reversing the DHT-induced serum FT, LH, and FSH concentrations (*Figure 3B*,*3D*,*3E*) and ovarian polycystic morphology (*Figure 4B*). In addition, both metformin and Diane-35 ameliorated the DHT-induced decrease in uterine and ovarian indices (*Figure 4A*,*4C-4E*), although the effect of Diane-35 surpassed that of metformin. These data indicate that Diane-35 and metformin play therapeutic roles in

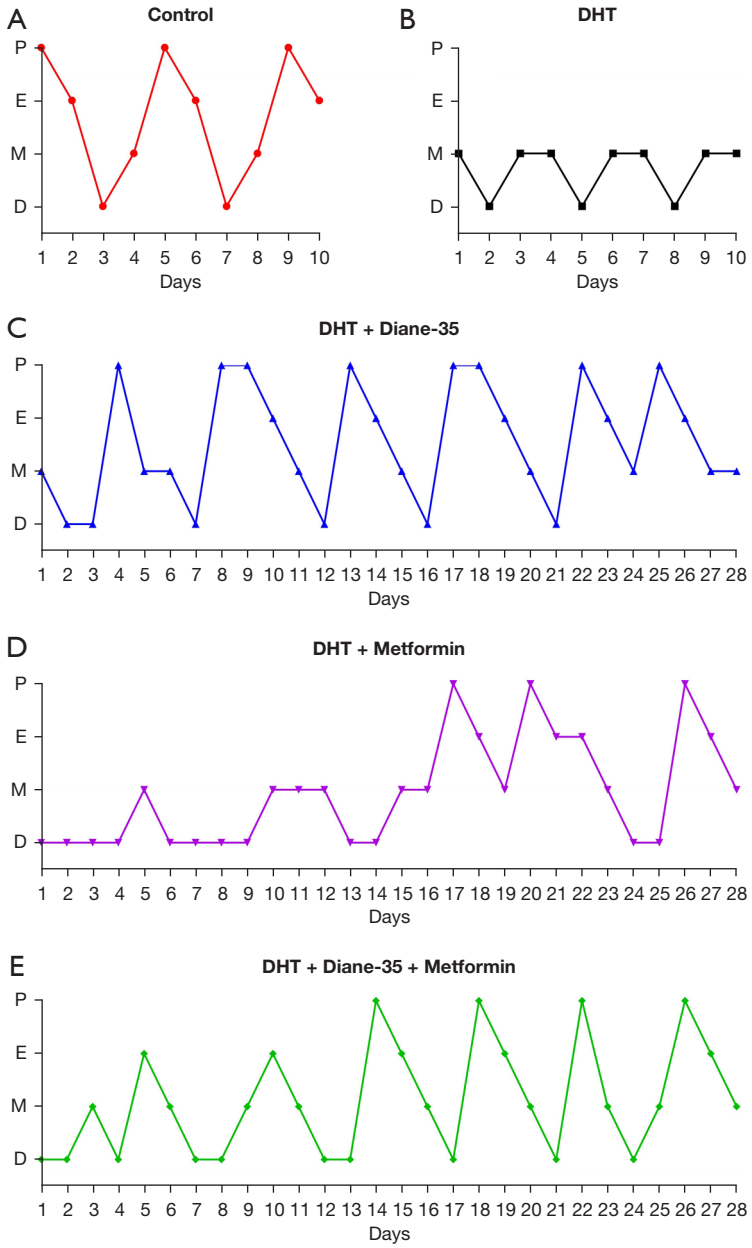

Figure 1 Representative estrous cycles of the 5 groups (A-E). Estrous stages are represented by lines indicating proestrus (P), estrus (E), metestrus (M), and diestrus (D) on the ordinate axis and the date on the abscissa axis. All line charts are representative of 3 independent experiments with similar results. DHT, dihydrotestosterone.

hyperandrogenemia, insulin resistance, and hypothalamus-pituitary-ovary (HPO) axis disruption in the PCOS model.

Diane-35 and metformin mediated reversal of endometrial hyperplasia

To explore the effects of high-concentration androgen treatment and combined treatment on the local endometrium, the DAPI-labeled region (endometrium and myometrium) was reconstructed using Imaris software, and the average volume of these different regions was calculated (*Figure 5A*). DHT modeling promoted uterine atrophy, leading to a significant decrease in the absolute volume of the endometrium and myometrium (*Figure 5B,5C*). In

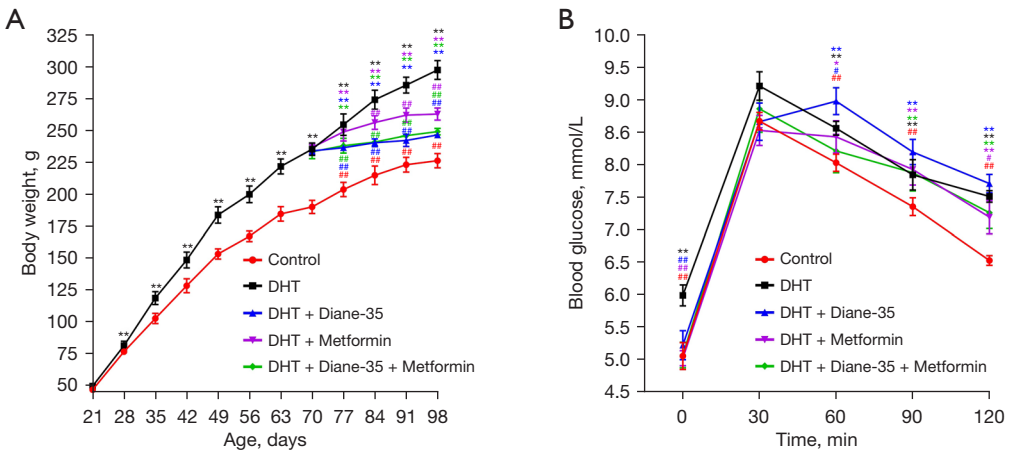

Figure 2 Growth curves and OGTT results of rats. (A) Growth curves of rats. From 0 days to 84 days after the DHT tube implantation, body weight was recorded every 7 days (n=6 rats per group). (B) The OGTT results showed that the basal blood glucose level was measured before the administration of oral D-glucose (2 g/kg). Measurements were made at 30, 60, 90, and 120 min (n=6 rats per group). *, P<0.05 compared to the control group; **, P<0.01 compared to the control group; #, P<0.05 compared to the DHT group; ##, P<0.05 compared to the DHT group. DHT, dihydrotestosterone; OGTT, oral glucose tolerance test.

contrast, treatment with Diane-35 and metformin improved the DHT-induced endometrial atrophy (*Figure 5B*). Regarding the absolute volume of the myometrium, there was no significant difference (*Figure 5C*). By calculating the endometrium: myometrium volume ratio, we found that this ratio increased after treatment and that this increase was weakened or even reversed by Diane-35 and metformin (*Figure 5D*).

To explore the impact of the DHT, Diane-35, and metformin treatments on endometrial glands, we used Imaris for the 3D reconstruction of DAPI-labeled glands and statistical analysis of the average gland volume in these different groups (*Figure 6A*). Although the absolute volume of glands between the control group and the remaining 4 groups was not significantly different (*Figure 6B*), DHT treatment increased the gland to endometrium ratio (*Figure 6C*).

The expression of AR and GLUT4 in the endometrium

To study the effect of hyperandrogenism and insulin resistance on the endometrium, AR and GLUT4 antibodies were used to immunolabel the 3D specimens in order to locate and quantify AR and GLUT4 expression (*Figure 7*). The images show AR and GLUT4 colocalization in the endometrium and their possible interaction (Figure S4A,S4B; Video S2). Both AR and GLUT4 were localized to epithelial and stromal tissues (*Figure 7A*). By measuring the AR and GLUT4 fluorescence signals via Imaris, we calculated all the fluorescence intensities in different areas of the endometrium and compared the data of the other 4 groups with those of the control group. The results showed that, compared with that after the control treatment, the DHT treatment decreased GLUT4 and that this decrease was especially significant in the endometrium and epithelium (*Figure 7B,7C*). Results also revealed that DHT tended to increase AR expression in all parts (*Figure 7E-7G*) and decrease GLUT4 in the stroma. Diane-35 treatment downregulated AR expression significantly in the endometrium and epithelium (*Figure 7E,7F*) but not in the stroma (*Figure 7G*). After metformin treatment, the expression of GLUT4 in both the epithelium and stroma was increased (*Figure 7C,7D*), while AR expression was decreased only in the stroma (*Figure 7G*). After the combined treatment with Diane-35 and metformin, GLUT4 expression increased in both the endometrium and stroma (*Figure 7B,7D*). Additionally, the expression of AR in all areas was significantly decreased (*Figure 7E-7G*), and this effect was confirmed in both epithelial and stromal tissues (*Figure 7F,7G*).

Discussion

Patients with PCOS are considered to be at higher risk of developing EC (34). Current studies have revealed that anovulation in patients with PCOS, which provides a long-term estrogen stimulation environment without the effects

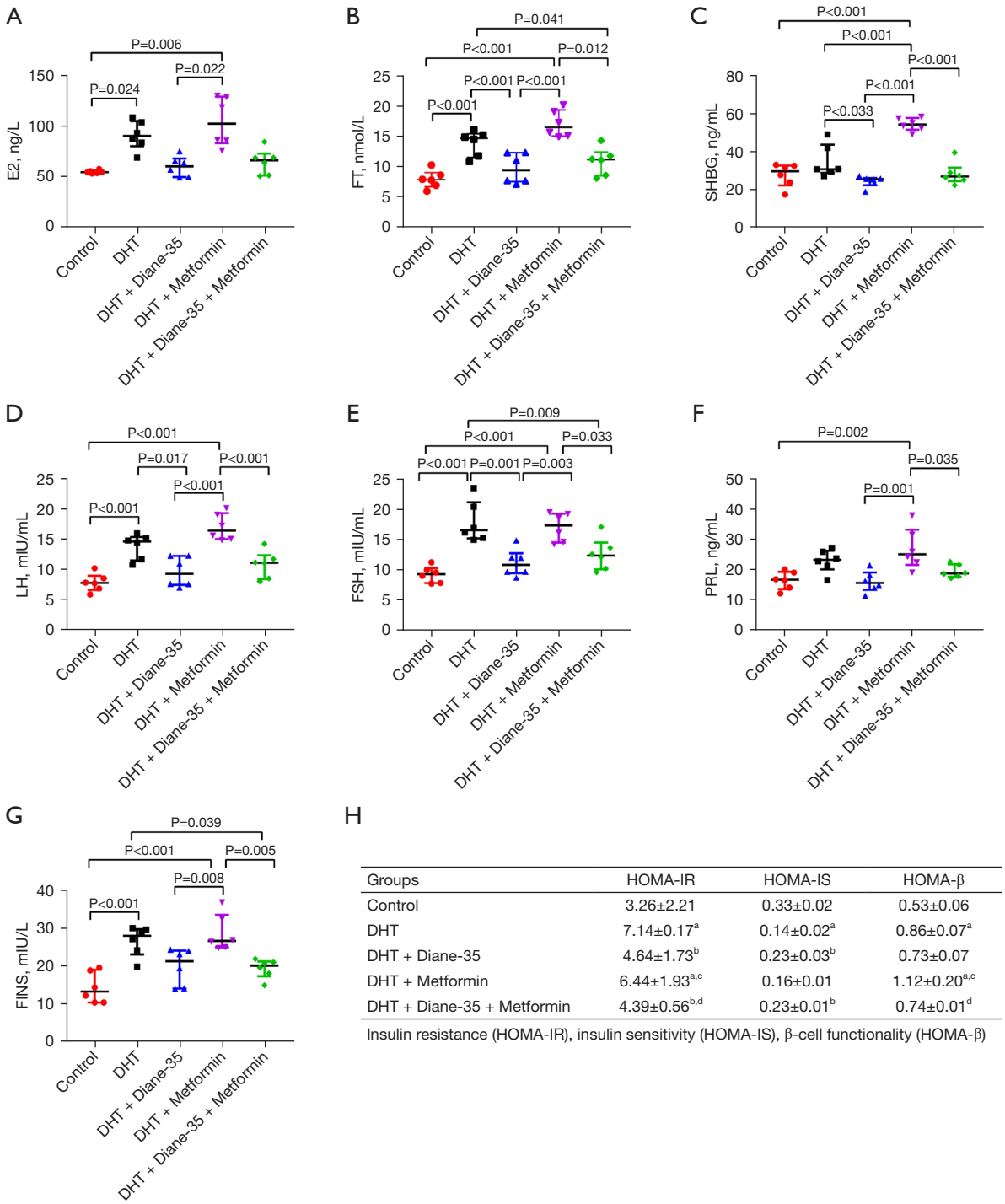

H

Groups	HOMA-IR	HOMA-IS	HOMA-β
Control	3.26±2.21	0.33±0.02	0.53±0.06
DHT	7.14±0.17[a]	0.14±0.02[a]	0.86±0.07[a]
DHT + Diane-35	4.64±1.73[b]	0.23±0.03[b]	0.73±0.07
DHT + Metformin	6.44±1.93[a,c]	0.16±0.01	1.12±0.20[a,c]
DHT + Diane-35 + Metformin	4.39±0.56[b,d]	0.23±0.01[b]	0.74±0.01[d]

Insulin resistance (HOMA-IR), insulin sensitivity (HOMA-IS), β-cell functionality (HOMA-β)

Figure 3 Eight hormone profiles and biochemical indices were assessed. (A) Levels of E2. (B) Levels of FT. (C) Levels of SHBG. (D) Levels of LH. (E) Levels of FSH. (F) Levels of PRL. (G) Levels of FINS. (H) HOMA-IR, HOMA-IS, and HOMA-β for the 5 groups of rats (n=6 rats per group). [a], P<0.05 compared to the control group; [b], P<0.05 compared to the DHT group; [c], P<0.05 compared to the DHT + Diane-35 group; [d], P<0.05 compared to the DHT + metformin group. DHT, dihydrotestosterone; E2, estradiol; FT, free testosterone; SHBG, sex hormone-binding globulin; LH, luteinizing hormone; FSH, follicle-stimulating hormone; PRL, prolactin; FINS, fasting insulin; HOMA-IR, homeostasis model assessment of insulin resistance; HOMA-IS, homeostasis model assessment of insulin sensitivity; HOMA-β, homeostasis model assessment of β-cell function.

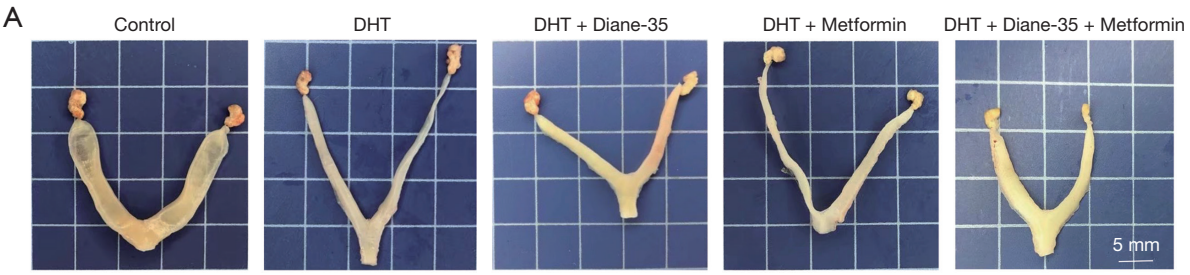

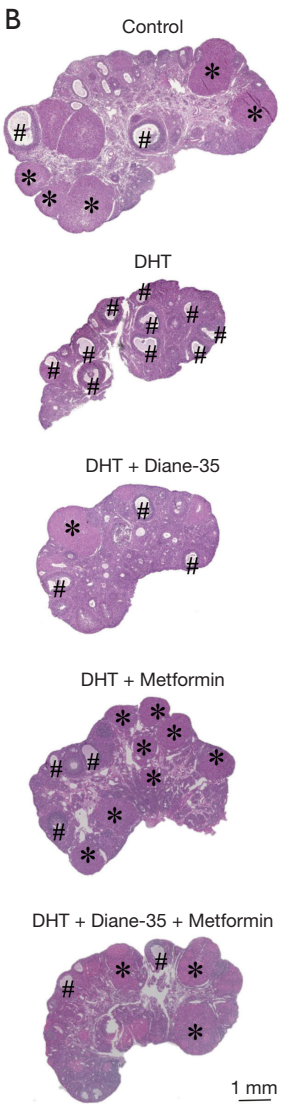

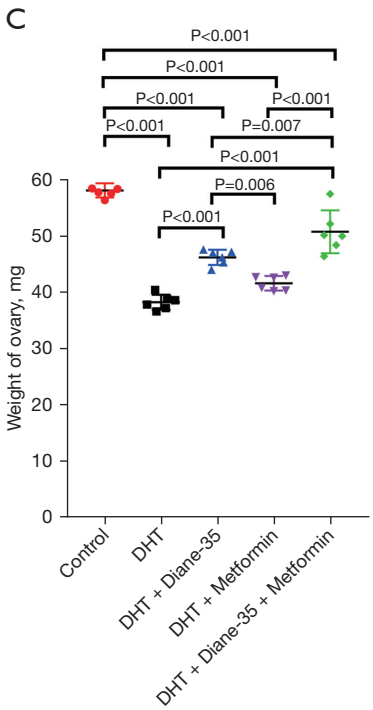

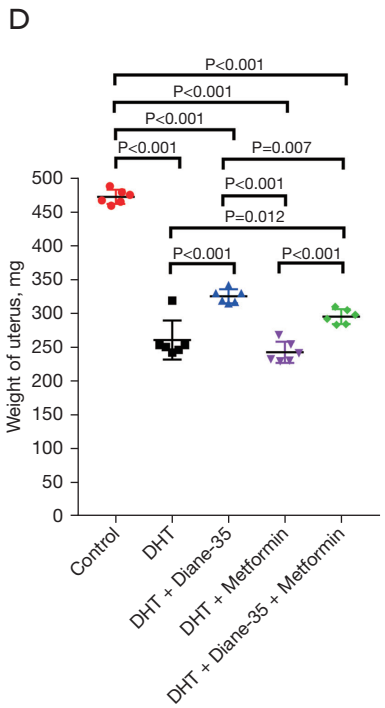

E

Groups	Ovary index (mg/100g)	Uterus index (mg/100g)
Control	25.00±1.78	205.96±73.97
DHT	12.11±1.98[a]	87.49±57.96[a]
DHT + Diane-35	19.73±3.16[a,b]	132.80±32.09[a,b]
DHT + Metformin	16.71±2.07[a,b,c]	94.07±56.14[a,c]
DHT + Diane-35 + Metformin	20.31±3.28[a,b,d]	119.37±46.89[a,b,c,d]

Ovary index = ovary weight (mg) body weight (100g); Uterus index = uterus weight (mg)/body weight (100 g)
[a]P<0.05 significance against Control
[b]P<0.05 significance against DHT
[c]P<0.05 significance against DHT + Diane-35
[d]P<0.05 significance against DHT + Metformin

Figure 4 Morphology and gonadosomatic index of uteri and ovaries. (A) Morphology of uteri and ovaries (scale bars: 5 mm). Images are representative of 6 independent experiments with similar results. (B) Hematoxylin and eosin staining of ovaries (scale bars: 1 mm). Images are representative of 3 independent experiments with similar results. The cystic follicle is indicated by a hash symbol (#), while the corpora lutea are indicated by asterisks (*). (C) Ovarian weight, (D) uterine weight, and (E) gonadosomatic index of the uteri and ovaries for 5 groups of rats (n=6 rats per group). [a], P<0.05 compared to the control group; [b], P<0.05 compared to the DHT group; [c], P<0.05 compared to the DHT + Diane-35 group; [d], P<0.05 compared to the DHT + metformin group. DHT, dihydrotestosterone.

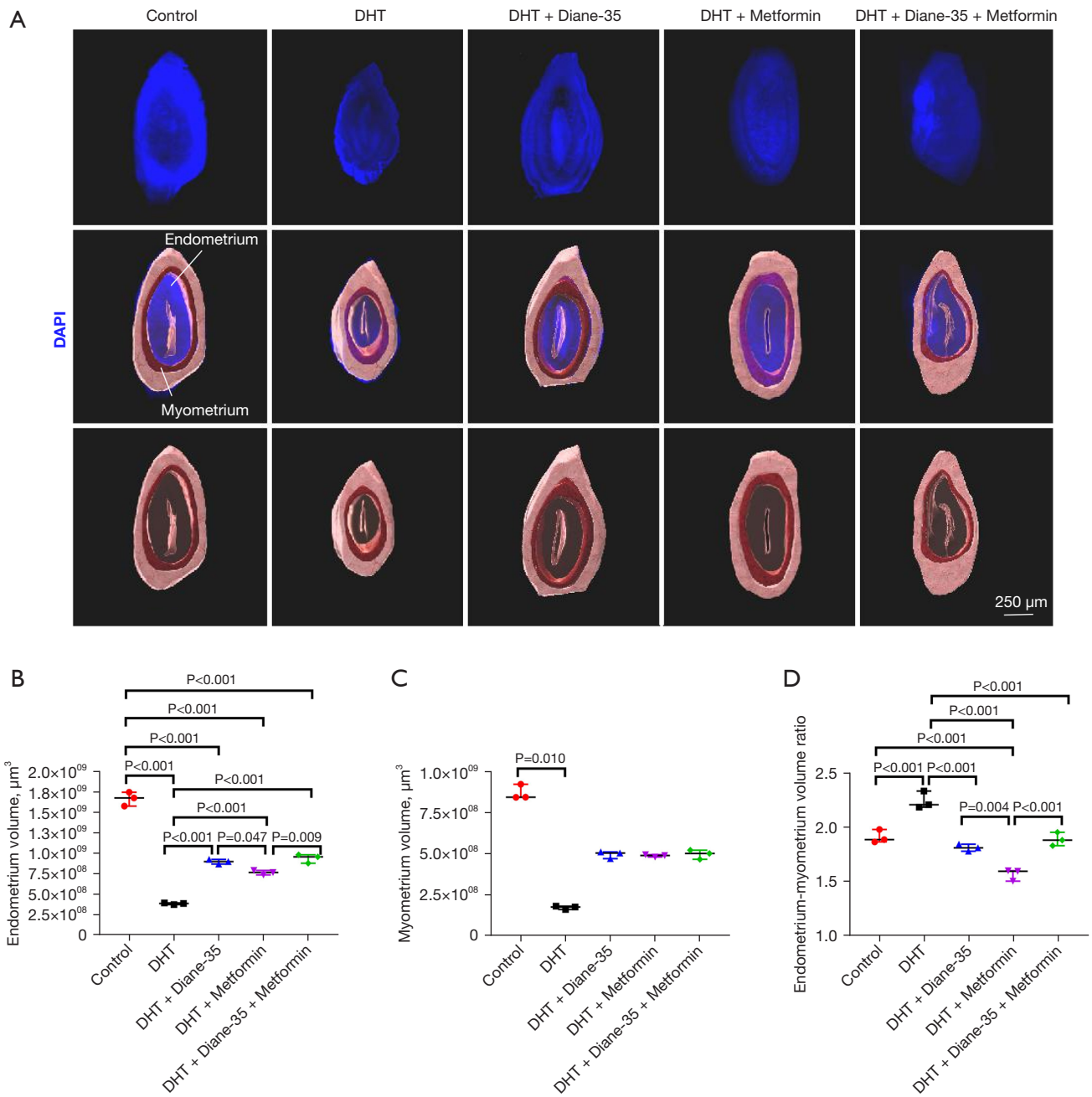

Figure 5 Treatment ameliorated DHT-induced endometrial hyperplasia. (A) Uteri were immune-stained with DAPI (blue) (scale bars: 250 μm). First row: three-dimensional rendered images of the whole uterus. Second row: reconstructed images of the DAPI-stained 3-layer structure. Third row: three-layer structure images of the uteri. (B-D) Quantification of the absolute volume of the endometrium (B) and myometrium (C) and their ratio (D). Images are representative of 3 independent experiments with similar results. DHT, dihydrotestosterone; DAPI, 4',6-diamidino-2-phenylindole.

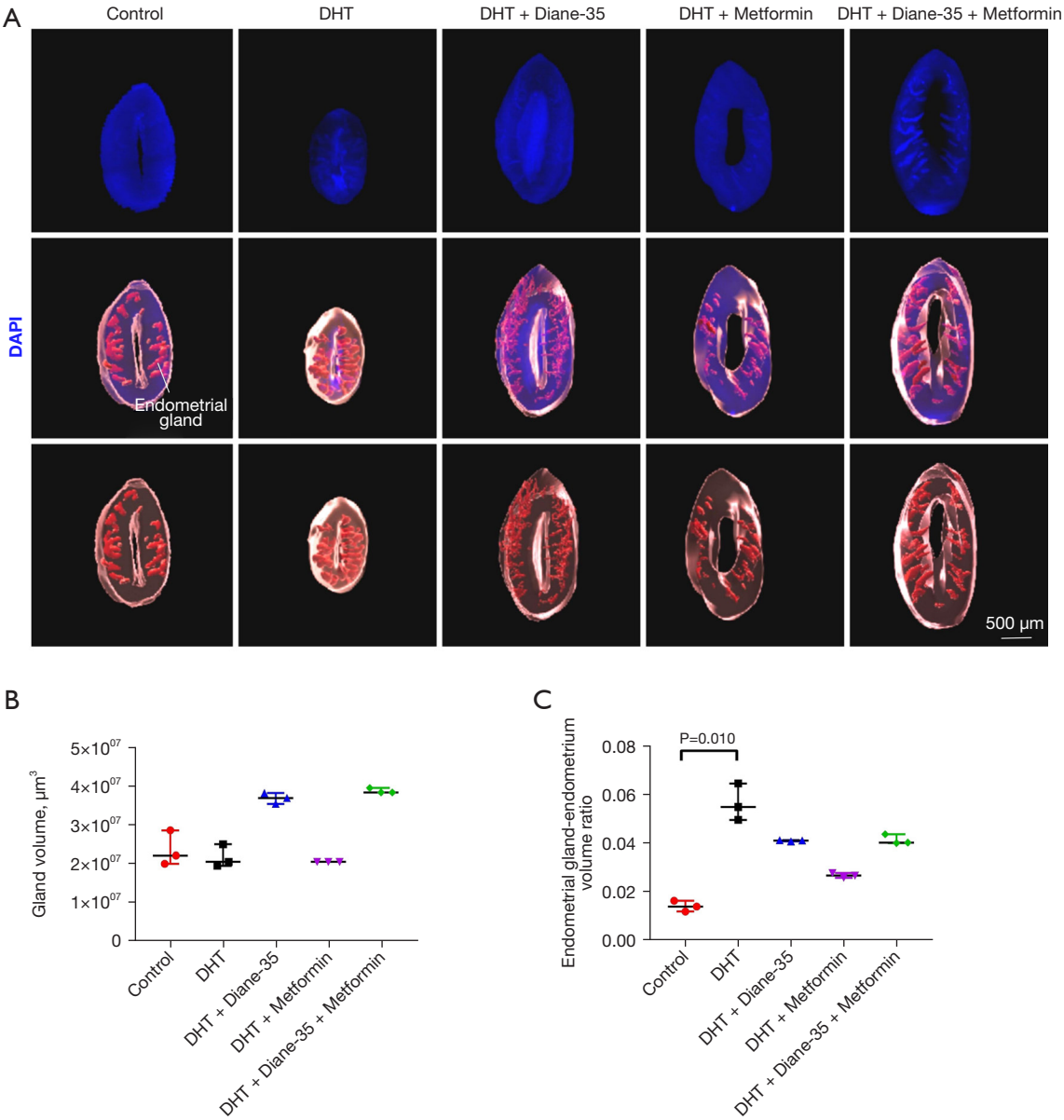

Figure 6 Treatment ameliorated DHT-induced uterine gland formation. (A) Reconstruction of endometrial glands (scale bars: 500 μm). Upper row: three-dimensional rendering images of the endometrium. Middle row: reconstruction images of the endometrial glands. Lower row: the endometrial glands in the endometrium. (B) Quantification of the absolute volume of endometrial glands. (C) Gland/endometrium volume ratio. Images are representative of 3 independent experiments with similar results. DHT, dihydrotestosterone; DAPI, 4',6-diamidino-2-phenylindole.

of progesterone on the endometrium, leads to a high prevalence of EC in these patients (35,36). In addition, insulin resistance and hyperandrogenemia, which are characteristic of PCOS, have been associated with a high risk of EC in patients with PCOS (37,38). The European Prospective Investigation on Cancer and Nutrition Into Cancer and Nutrition (EPIC) cohort study identified a cluster of factors associated with EC risk, including insulin resistance/metabolic syndrome, steroid hormones, and inflammatory factors (38,39). Although there are many studies focusing on the effects of progesterone and estrogen on EC, few studies have focused on the function of

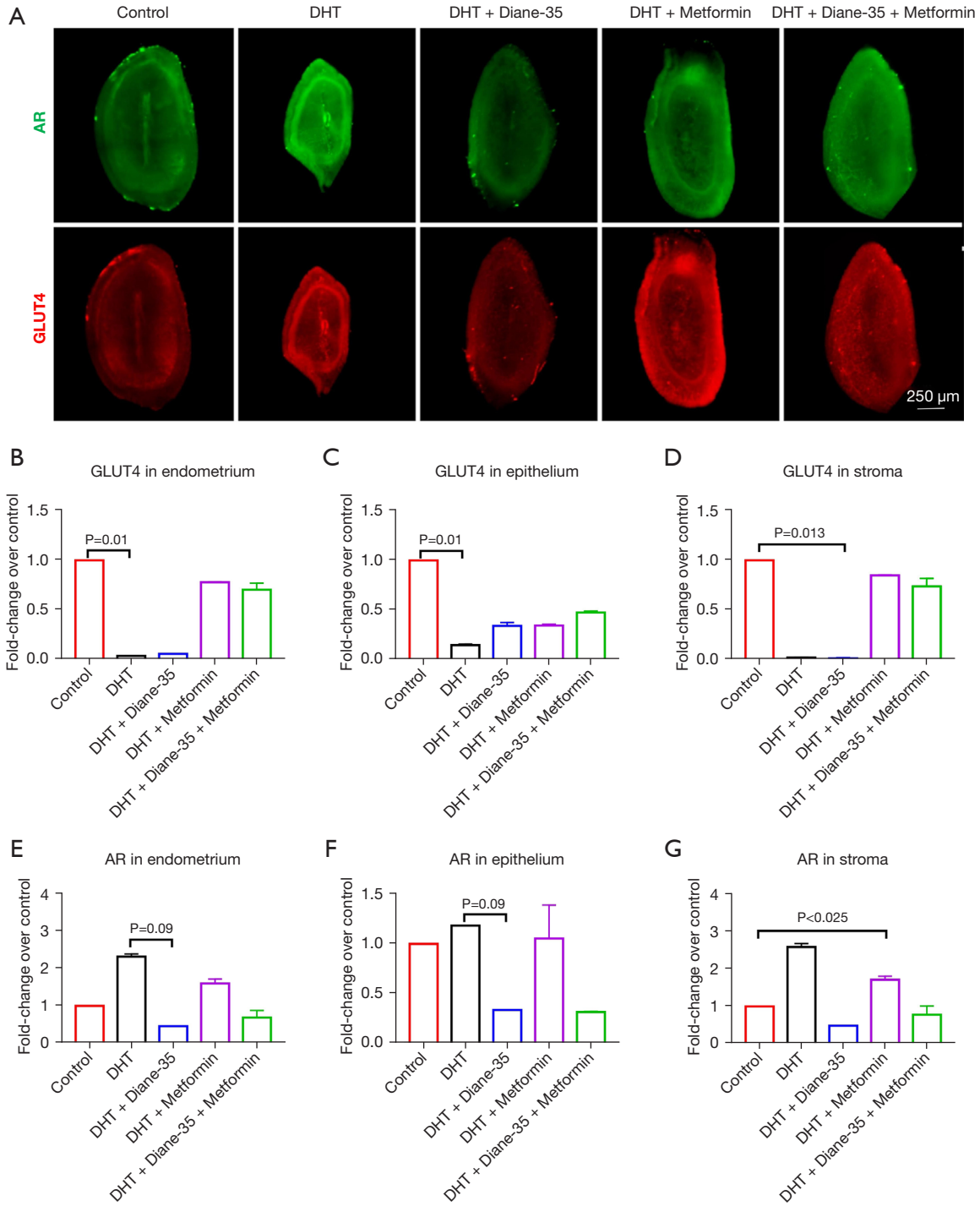

Figure 7 Anti-hyperandrogenism and insulin-sensitizing therapy reversed DHT-induced increases in AR expression and decreases in GLUT4 expression. (A) Uteri from 5 groups were immune-stained with specific antibodies. First row: AR (green); second row: GLUT4 (red). Quantification of the relative fluorescence intensity of GLUT4 in the endometrium (B), the epithelium (C), and the stroma (D). Quantification of the relative fluorescence intensity of AR in the endometrium (E), the epithelium (F), and the stroma (G). Images are representative of 3 independent experiments with similar results. DHT, dihydrotestosterone; AR, androgen receptor; GLUT4, glucose transportation protein 4.

androgen and insulin while the relationship among insulin resistance, hyperandrogenism, and EC morbidity remains poorly understood.

This study investigated the effects of hyperandrogenemia and insulin resistance on the endometrium and further explored the effect of Diane-35 and metformin treatment on PCOS-related EC. The results showed that DHT treatment beginning in prepuberty resulted in significant hyperandrogenemia and insulin resistance in rats. In addition, long-term DHT stimulation caused other obvious PCOS characteristics, including polycystic ovarian morphology, disrupted HPO axis regulation, and relative endometrial hyperplasia. The DHT-induced symptoms were ameliorated by treatment with Diane-35, metformin, and their combination. Diane-35 exerted a strong antiandrogenic effect, while metformin seemed to play an important role in improving glucose metabolism. Although the synergistic effect of Diane-35 and metformin remains to be further explored, our study has preliminarily elucidated their role in regulating AR and GLUT4 expression. The endometrium is composed of many cell types, including epithelial and stromal cells. The expression of AR and GLUT4 in different cell types is closely related to endometrial status. To explore the interaction between endometrial lesions and AR, GLUT4 expression was measured under conditions of hyperandrogenemia and insulin resistance. We used a 3D imaging technique to analyze segments of the uterus. With this technique, we could analyze samples on a large scale via fluorescent labeling, which facilitated the analysis of the changes in tissue structures and key factors.

Here, we report that continuous DHT stimulation led to a PCOS-like appearance characterized by increased body weight, disordered hormone levels, and polycystic ovary morphology. Additionally, treatment with metformin and Diane-35 alleviated the syndromes mentioned above. Long-term DHT treatment resulted in hyperandrogenism and hyperinsulinemia in rats. These processes regulated the compartment-specific expression of AR and GLUT4 in the endometrium and finally contributed to a compartment-specific increase in the volume of the endometrium and uterine glands. These results are consistent with the phenomenon of increased risk of EC and endometrial atypical hyperplasia (EAH) in patients with PCOS with hyperandrogenism and insulin resistance. These striking findings suggest a role for androgen and insulin in regulating endometrial homeostasis and the value of metformin and Diane-35 in the treatment of PCOS-related EAH and EC.

Androgens can be secreted by ovaries, adrenal glands, and other tissues in the female body. Androgens mainly include DHT, testosterone (T), androstenedione (A4), and dehydroepiandrosterone (DHEA). Androgens perform their functions by binding to AR. DHT and T have higher binding affinities for AR than DHEA and dehydroepiandrosterone sulfate (DHEAS), with DHT having the highest binding affinity (40). Androgen and AR are essential to female reproduction and are widely expressed throughout the female reproductive system, including in the endometrium (41,42). By binding to AR, androgens can regulate gene transcription in the nucleus and form estrogen by aromatization. In addition, the AMP-activated protein kinase (AMPK) signaling pathway may participate in this process (43). However, DHT is not affected by aromatase and cannot be converted into estrogen. AR is expressed in the female endometrium throughout the menstrual cycle. The expression of AR in the endometrial stroma and myometrium is higher than that in gland cells (42). AR expression in the proliferative stage is significantly higher than that in the secretory stage. In particular, the AR expression level is highest in stromal cells. AR expression remains positive in stromal cells throughout the menstrual cycle, while in the glandular epithelium, AR immunoactivity increases in the middle and late stages of secretion (42). AR plays an important role in the occurrence and development of sex hormone-dependent tumors. Some studies have indicated that androgen can mediate the overactivation of the phosphatidylinositol-4,5-bisphosphate3-kinase-protein kinase B (PI3K/Akt) signaling pathway and thus promote the proliferation of ovarian cancer cells in an AR-dependent manner (44). In addition, AR is highly expressed in breast cancer and has carcinogenic potential in ERα-negative breast cancer. However, AR exerts a potential tumor-suppressing effect in ERα-positive breast cancer, which may be due to the different regulatory mechanisms (45). The role of AR in prostate cancer is relatively well-studied. To date, various androgen antagonists have been used to treat prostate cancer, but chemoresistance after long-term treatment is the most severe challenge (46). This phenomenon may be related to the abnormal activation of AR in chemoresistant patients (47). However, the function of androgens in the endometrium is still controversial. This study reveals that androgens promote endometrial hyperplasia, which is similar to the results reported by Simitsidellis *et al.* (19) and Choi *et al.* (48). Androgens may play a direct role in endometrial hyperplasia and EC formation. However, the role of

androgens in endometrial hyperplasia and the occurrence and development of EC remain to be studied in the future.

Patients with PCOS have tissue-specific insulin resistance due to reduced insulin-IR binding and receptor-mediated pathway inactivation, which leads to increased compensatory insulin secretion (4,49). Glucose metabolism is closely related to the regulation of glucose transporters (GLUTs). Among these transporters, GLUT4 plays an important role in glucose metabolism under physiological and pathological conditions such as insulin resistance. For example, GLUT4 participates in endometrial hyperplasia and decidualization (50,51). Previously, tissue-specific insulin resistance was confirmed to exist in muscle, fat, and the liver, among other tissues. Some studies have confirmed that the endometrium also exhibits insulin resistance (52,53). GLUT4 shows periodic changes in the normal endometrium, with increased expression during the proliferative phase compared with that during the secretory phase. The expression level of GLUT4 in the endometrium is lower in women with PCOS and endometrial carcinoma and exhibits no significant periodic changes (54). GLUT4 expression is regulated by steroid hormones. With the regulation of progesterone, GLUT4 expression is decreased, whereas the combined use of estrogen improves chemoresistance to progesterone (54). This may provide insight into the mechanism underlying the chemoresistance to progesterone caused by long-term treatment with progesterone and the reason for the superior effect of Diane-35 over that of MPA. Many studies have shown that metformin can improve GLUT4 expression and regulate downstream IR-mTOR pathway activation (55).

In this research, vaginal smears indicated the levels of sex hormones and the changes in these levels in the body. The recovery of periodic estrous cycle changes demonstrated that sex hormone disorder in rats with high androgen levels could be corrected to a certain extent; in particular, HPO axis regulation could be normalized (56). The results of this part of our study are similar to those of Zhang *et al.* (52) and Sara *et al.* (57). Diane-35 and metformin were responsible for inhibiting androgen-induced weight gain. Diane-35 had a more significant effect, which may be due to its strong antiandrogenic effect (58). The effect of antiandrogen therapy on weight loss has been reported in several studies (14,59). The effects of metformin on weight loss are related mainly to its role in glucose metabolism regulation (57,60). Diane-35 and metformin have been clinically proven to improve PCOS (61). However, while Diane-35 has been shown to stimulate ovulation in some studies, it has also been demonstrated to be an effective contraceptive in humans. The role of Diane-35 in inducing ovulation in rats remains to be further discussed, and this effect may be related to the improvement of glycolysis (57). This study focuses on endometrial hyperplasia and cancer under the conditions of hyperandrogenism and insulin resistance, so the endometrium-related regulation of reproductive function was not explored. However, further analysis may be possible in future research (14,48,62,63). Because androgen/AR and insulin/GLUT4 play important roles in the endometrium, exploring their interaction and their downstream mechanisms are of particular importance.

Conclusions

In summary, we found that long-term DHT-mediated murine hyperandrogenism, insulin resistance and relative endometrial hyperplasia can be alleviated by metformin and Diane-35 combination treatment by regulating the expression of AR and GLUT4. Our results support Diane-35 and metformin as a combined therapy to treat PCOS and PCOS-related endometrial lesion.

Acknowledgments

We thank Min Jiang and Ying Shi of the Center Imaging at the Institutes of Brain Science, Fudan University, for the use of technical equipment and support. We thank Linus Shao for editing our manuscript.

Funding: This work was supported by the National Natural Science Foundation of China (No. 81572555), the Shanghai Committee of Science and Technology, China (No. 15411964700 to X.L.), and the National Natural Science Foundation of China (No. 81673766 to Y.F.).

Footnote

Reporting Checklist: The authors have completed the ARRIVE reporting checklist. Available at https://atm.amegroups.com/article/view/10.21037/atm-21-2441/rc

Data Sharing Statement: Available at https://atm.amegroups.com/article/view/10.21037/atm-21-2441/dss

Peer Review File: Available at https://atm.amegroups.com/article/view/10.21037/atm-21-2441/prf

Conflicts of Interest: All authors have completed the ICMJE

uniform disclosure form (available at https://atm.amegroups.com/article/view/10.21037/atm-21-2441/coif). YF reports funding support from the National Natural Science Foundation of China (No. 81673766). XL reports funding support from the National Natural Science Foundation of China (No. 81572555) and the Shanghai Committee of Science and Technology, China (No. 15411964700). The other authors have no conflicts of interest to declare.

Ethical Statement: The authors are accountable for all aspects of the work and for ensuring that questions related to the accuracy or integrity of any part of the work are appropriately investigated and resolved. All experimental procedures performed on rats were conducted in compliance with the Management Rule of Laboratory Animals (Chinese Order No. 676 of the State Council, revised 1 March 2017). This study was approved by the Animal Ethics Committee, School of Basic Medical Sciences of Fudan University, China.

References

1. Lizneva D, Suturina L, Walker W, et al. Criteria, prevalence, and phenotypes of polycystic ovary syndrome. Fertil Steril 2016;106:6-15.
2. Li R, Zhang Q, Yang D, et al. Prevalence of polycystic ovary syndrome in women in China: a large community-based study. Hum Reprod 2013;28:2562-9.
3. Milman LW, Dokras A. Long-Term Morbidity: Cardiovascular Disease, Cancer, and Depression in PCOS. Springer, New York; 2014.
4. Barry JA, Azizia MM, Hardiman PJ. Risk of endometrial, ovarian and breast cancer in women with polycystic ovary syndrome: a systematic review and meta-analysis. Hum Reprod Update 2014;20:748-58.
5. Haoula Z, Salman M, Atiomo W. Evaluating the association between endometrial cancer and polycystic ovary syndrome. Hum Reprod 2012;27:1327-31.
6. Gompel A. Progesterone and endometrial cancer. Best Pract Res Clin Obstet Gynaecol 2020;69:95-107.
7. Morice P, Leary A, Creutzberg C, et al. Endometrial cancer. Lancet 2016;387:1094-108.
8. Li X, Guo YR, Lin JF, et al. Combination of Diane-35 and Metformin to Treat Early Endometrial Carcinoma in PCOS Women with Insulin Resistance. J Cancer 2014;5:173-81.
9. Zhao S, Li G, Yang L, et al. Response-specific progestin resistance in a newly characterized Ishikawa human endometrial cancer subcell line resulting from long-term exposure to medroxyprogesterone acetate. Oncol Lett 2013;5:139-44.
10. Aghajanova L, Velarde MC, Giudice LC. Altered gene expression profiling in endometrium: evidence for progesterone resistance. Semin Reprod Med 2010;28:51-8.
11. Sanchez-Rangel E, Inzucchi SE. Metformin: clinical use in type 2 diabetes. Diabetologia 2017;60:1586-93.
12. Bitzer J, Römer T, Lopes da Silva Filho A. The use of cyproterone acetate/ethinyl estradiol in hyperandrogenic skin symptoms - a review. Eur J Contracept Reprod Health Care 2017;22:172-82.
13. Cui N, Feng X, Zhao Z, et al. Restored Plasma Anandamide and Endometrial Expression of Fatty Acid Amide Hydrolase in Women With Polycystic Ovary Syndrome by the Combination Use of Diane-35 and Metformin. Clin Ther 2017;39:751-8.
14. Li Y, Ruan X, Wang H, et al. Comparing the risk of adverse pregnancy outcomes of Chinese patients with polycystic ovary syndrome with and without antiandrogenic pretreatment. Fertil Steril 2018;109:720-7.
15. Dehdashti F, Wu N, Ma CX, et al. Association of PET-based estradiol-challenge test for breast cancer progesterone receptors with response to endocrine therapy. Nat Commun 2021;12:733.
16. Cho A, Lee SW, Park JY, et al. Continued medical treatment for persistent early endometrial cancer in young women. Gynecol Oncol 2021;160:413-7.
17. Burchardt NA, Shafrir AL, Kaaks R, et al. Oral contraceptive use by formulation and endometrial cancer risk among women born in 1947-1964: The Nurses' Health Study II, a prospective cohort study. Eur J Epidemiol 2021;36:827-39.
18. Saguyod SJU, Alhallak I, Simmen RCM, et al. Metformin regulation of progesterone receptor isoform-B expression in human endometrial cancer cells is glucose-dependent. Oncol Lett 2020;20:249.
19. Simitsidellis I, Gibson DA, Cousins FL, et al. A Role

for Androgens in Epithelial Proliferation and Formation of Glands in the Mouse Uterus. Endocrinology 2016;157:2116-28.
20. Noroozzadeh M, Behboudi-Gandevani S, Zadeh-Vakili A, et al. Hormone-induced rat model of polycystic ovary syndrome: A systematic review. Life Sci 2017;191:259-72.
21. Zhang F, Ma T, Cui P, et al. Diversity of the Gut Microbiota in Dihydrotestosterone-Induced PCOS Rats and the Pharmacologic Effects of Diane-35, Probiotics, and Berberine. Front Microbiol 2019;10:175.
22. Huang K, Walker CA. Comparisons of statistical models for growth curves from 90-day rat feeding studies. Arch Toxicol 2019;93:2397-408.
23. Byers SL, Wiles MV, Dunn SL, et al. Mouse estrous cycle identification tool and images. PLoS One 2012;7:e35538.
24. Cora MC, Kooistra L, Travlos G. Vaginal Cytology of the Laboratory Rat and Mouse: Review and Criteria for the Staging of the Estrous Cycle Using Stained Vaginal Smears. Toxicol Pathol 2015;43:776-93.
25. Shorr E. A New Technic for Staining Vaginal Smears: III, A Single Differential Stain. Science 1941;94:545-6.
26. Ghezzi AC, Cambri LT, Botezelli JD, et al. Metabolic syndrome markers in wistar rats of different ages. Diabetol Metab Syndr 2012;4:16.
27. Yan Y, Xu Q, Zhao C, et al. In vivo pharmacokinetic study and oral glucose tolerance test of sulfoxide analogs of GPR40 agonist TAK-875. Drug Dev Res 2020;81:708-15.
28. Zhang WL, Liu SH, Zhang WC, et al. Skeletal Muscle CLARITY: A Preliminary Study of Imaging The Three-Dimensional Architecture of Blood Vessels and Neurons. Cell J 2018;20:132-7.
29. Ma T, Cui P, Tong X, et al. Endogenous Ovarian Angiogenesis in Polycystic Ovary Syndrome-Like Rats Induced by Low-Frequency Electro-Acupuncture: The CLARITY Three-Dimensional Approach. Int J Mol Sci 2018;19:3500.
30. Wang H, Lu Y, Yan Y, et al. Promising Treatment for Type 2 Diabetes: Fecal Microbiota Transplantation Reverses Insulin Resistance and Impaired Islets. Front Cell Infect Microbiol 2019;9:455.
31. Qi X, Yun C, Sun L, et al. Gut microbiota-bile acid-interleukin-22 axis orchestrates polycystic ovary syndrome. Nat Med 2019;25:1225-33.
32. Susaki EA, Tainaka K, Perrin D, et al. Advanced CUBIC protocols for whole-brain and whole-body clearing and imaging. Nat Protoc 2015;10:1709-27.
33. Renier N, Wu Z, Simon DJ, et al. iDISCO: a simple, rapid method to immunolabel large tissue samples for volume imaging. Cell 2014;159:896-910.
34. Kempegowda P, Melson E, Manolopoulos KN, et al. Implicating androgen excess in propagating metabolic disease in polycystic ovary syndrome. Ther Adv Endocrinol Metab 2020;11:2042018820934319.
35. Fortner RT, Hüsing A, Dossus L, et al. Theoretical potential for endometrial cancer prevention through primary risk factor modification: Estimates from the EPIC cohort. Int J Cancer 2020;147:1325-33.
36. Fearnley EJ, Marquart L, Spurdle AB, et al. Polycystic ovary syndrome increases the risk of endometrial cancer in women aged less than 50 years: an Australian case-control study. Cancer Causes Control 2010;21:2303-8.
37. Dashti SG, English DR, Simpson JA, et al. Adiposity and Endometrial Cancer Risk in Postmenopausal Women: A Sequential Causal Mediation Analysis. Cancer Epidemiol Biomarkers Prev 2021;30:104-13.
38. Fortner RT, Hüsing A, Kühn T, et al. Endometrial cancer risk prediction including serum-based biomarkers: results from the EPIC cohort. Int J Cancer 2017;140:1317-23.
39. Dossus L, Lukanova A, Rinaldi S, et al. Hormonal, metabolic, and inflammatory profiles and endometrial cancer risk within the EPIC cohort--a factor analysis. Am J Epidemiol 2013;177:787-99.
40. Cloke B, Christian M. The role of androgens and the androgen receptor in cycling endometrium. Mol Cell Endocrinol 2012;358:166-75.
41. Mertens HJ, Heineman MJ, Koudstaal J, et al. Androgen receptor content in human endometrium. Eur J Obstet Gynecol Reprod Biol 1996;70:11-3.
42. Li X, Pishdari B, Cui P, et al. Regulation of Androgen Receptor Expression Alters AMPK Phosphorylation in the Endometrium: In Vivo and In Vitro Studies in Women with Polycystic Ovary Syndrome. Int J Biol Sci 2015;11:1376-89.
43. Risch HA. Hormonal etiology of epithelial ovarian cancer, with a hypothesis concerning the role of androgens and progesterone. J Natl Cancer Inst 1998;90:1774-86.
44. Li Y, Li S, Zhang Y, et al. Androgen Plays a Carcinogenic Role in EOC via the PI3K/AKT Signaling Pathway in an AR-Dependent Manner. J Cancer 2021;12:1815-25.
45. Hickey TE, Robinson JL, Carroll JS, et al. Minireview: The androgen receptor in breast tissues: growth inhibitor, tumor suppressor, oncogene? Mol Endocrinol 2012;26:1252-67.
46. Mostaghel EA, Plymate S. New hormonal therapies for castration-resistant prostate cancer. Endocrinol Metab Clin North Am 2011;40:625-42, x.

47. Estébanez-Perpiñá E, Bevan CL, McEwan IJ. Eighty Years of Targeting Androgen Receptor Activity in Prostate Cancer: The Fight Goes on. Cancers (Basel) 2021;13:509.
48. Choi JP, Zheng Y, Skulte KA, et al. Development and Characterization of Uterine Glandular Epithelium Specific Androgen Receptor Knockout Mouse Model. Biol Reprod 2015;93:120.
49. Shafiee MN, Chapman C, Barrett D, et al. Reviewing the molecular mechanisms which increase endometrial cancer (EC) risk in women with polycystic ovarian syndrome (PCOS): time for paradigm shift? Gynecol Oncol 2013;131:489-92.
50. Liao Y, Huang R, Sun Y, et al. An inverse association between serum soluble receptor of advanced glycation end products and hyperandrogenism and potential implication in polycystic ovary syndrome patients. Reprod Biol Endocrinol 2017;15:9.
51. Wu XK, Zhou SY, Liu JX, et al. Selective ovary resistance to insulin signaling in women with polycystic ovary syndrome. Fertil Steril 2003;80:954-65.
52. Zhang Y, Sun X, Sun X, et al. Molecular characterization of insulin resistance and glycolytic metabolism in the rat uterus. Sci Rep 2016;6:30679.
53. Cui P, Li X, Wang X, et al. Lack of cyclical fluctuations of endometrial GLUT4 expression in women with polycystic ovary syndrome: Evidence for direct regulation of GLUT4 by steroid hormones. BBA Clin 2015;4:85-91.
54. Shao R, Li X, Feng Y, et al. Direct effects of metformin in the endometrium: a hypothetical mechanism for the treatment of women with PCOS and endometrial carcinoma. J Exp Clin Cancer Res 2014;33:41.
55. Estienne A, Bongrani A, Ramé C, et al. Energy sensors and reproductive hypothalamo-pituitary ovarian axis (HPO) in female mammals: Role of mTOR (mammalian target of rapamycin), AMPK (AMP-activated protein kinase) and SIRT1 (Sirtuin 1). Mol Cell Endocrinol 2021;521:111113.
56. Zhang S, Tu H, Yao J, et al. Combined use of Diane-35 and metformin improves the ovulation in the PCOS rat model possibly via regulating glycolysis pathway. Reprod Biol Endocrinol 2020;18:58.
57. Sara L, Antal P, Masszi G, et al. Arteriolar insulin resistance in a rat model of polycystic ovary syndrome. Fertil Steril 2012;97:462-8.
58. Ruan X, Song J, Gu M, et al. Effect of Diane-35, alone or in combination with orlistat or metformin in Chinese polycystic ovary syndrome patients. Arch Gynecol Obstet 2018;297:1557-63.
59. Olaniyi KS, Oniyide AA, Adeyanju OA, et al. Low dose spironolactone-mediated androgen-adiponectin modulation alleviates endocrine-metabolic disturbances in letrozole-induced PCOS. Toxicol Appl Pharmacol 2021;411:115381.
60. Wang T, Zhang J, Hu M, et al. Differential Expression Patterns of Glycolytic Enzymes and Mitochondria-Dependent Apoptosis in PCOS Patients with Endometrial Hyperplasia, an Early Hallmark of Endometrial Cancer, In Vivo and the Impact of Metformin In Vitro. Int J Biol Sci 2019;15:714-25.
61. Mhao NS, Al-Hilli AS, Hadi NR, et al. A comparative study to illustrate the benefits of using ethinyl estradiol-cyproterone acetate over metformin in patients with polycystic ovarian syndrome. Diabetes Metab Syndr 2016;10:S95-8.
62. Hu M, Zhang Y, Guo X, et al. Hyperandrogenism and insulin resistance induce gravid uterine defects in association with mitochondrial dysfunction and aberrant reactive oxygen species production. Am J Physiol Endocrinol Metab 2019;316:E794-809.
63. Zhang Y, Zhao W, Xu H, et al. Hyperandrogenism and insulin resistance-induced fetal loss: evidence for placental mitochondrial abnormalities and elevated reactive oxygen species production in pregnant rats that mimic the clinical features of polycystic ovary syndrome. J Physiol 2019;597:3927-50.

(English Language Editors: C. Mullens and J. Gray)

Cite this article as: Liu Y, Xu R, Zhou Y, Wang Y, Zhang F, Tong X, Cui P, Ma T, Sun J, Feng Y, Li X. Diane-35 and metformin therapy in rats with endometrial lesions induced by dihydrotestosterone exposure. Ann Transl Med 2023;11(6):247. doi: 10.21037/atm-21-2441

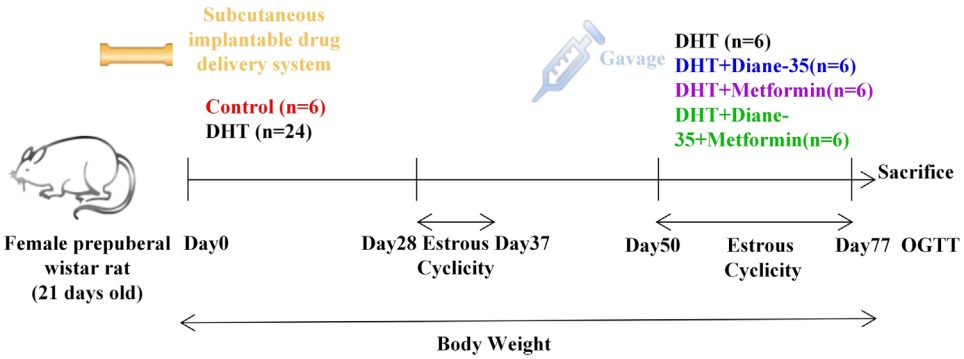

Figure S1 Timeline for the rat subjected to Diane-35, metformin, and combined treatment after DHT administration. Twenty-one-day-old female Wistar rats were randomly divided into 2 groups as shown. The control group (n=6) and the DHT group (n=24) were implanted with subdermal Silastic tubes filled with or without DHT. After 7 weeks, the DHT-treated rats were separated into 4 groups and orally administered 1% sodium carboxymethyl cellulose solution of Diane-35, metformin, or the combination treatment of Diane-35 and metformin. The 4 groups were named according to the used drugs. DHT: dihydrotestosterone.

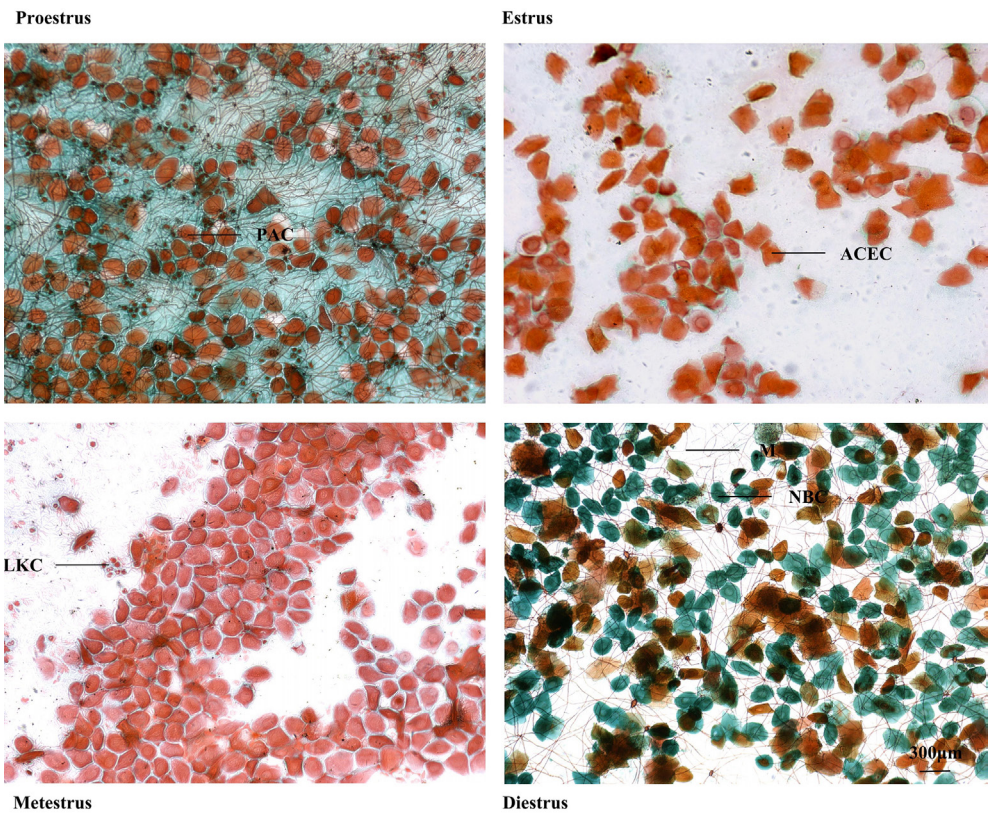

Figure S2 Representative estrous cycles. Cell types were identified by Shorr's staining, and every stage was distinguished by different cell proportions. Proestrus is characterized by preacidophilic cells (PACs), which include nucleated acidophilic cells (NACs) and enucleated acidophilic cells (EACs). Estrus contains mainly deciduously accumulated acidophilic cornified epithelial cells (ACECs), accompanied by a few EACs from the previous stage. Metestrus consists of clumps of EACs, NACs, and leukocytes (LKCs), and the ratio is close to 1:1:1. Diestrus consists of cornified epithelial cells (CECs), nucleated basophilic epithelial cells (NBCs), and a predominance of leukocytes (LKCs), usually coexisting with a large amount of mucus (M).

https://dx.doi.org/10.21037/atm-21-2441

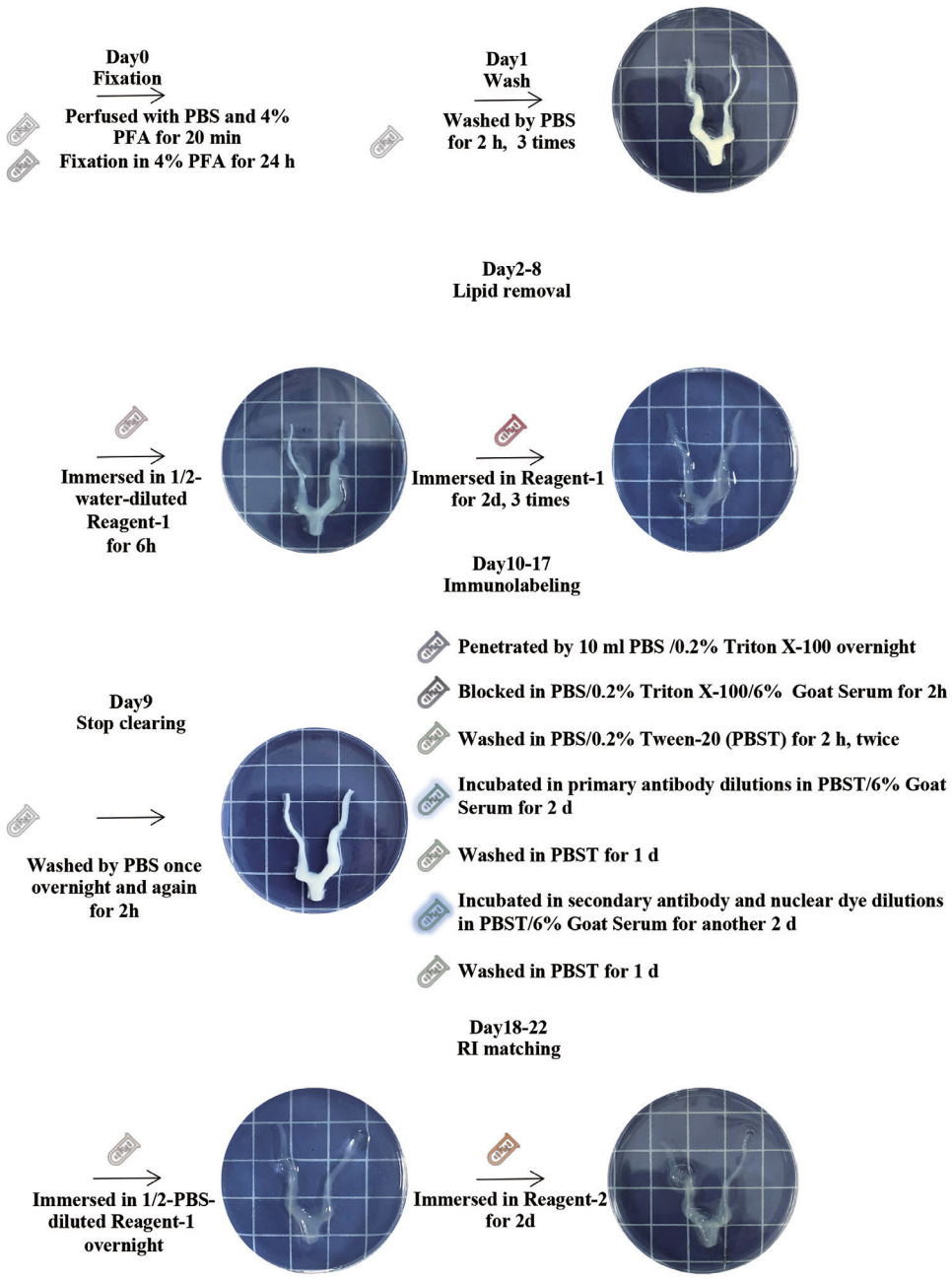

Figure S3 The tissue clearing and immunolabeling protocol. For the whole adult rat uterus, simple immersion and shaking in a 37 ℃ environment took approximately 10 days for thorough lipid removal and 7 days for immunolabeling. Then, it took approximately 4 days for refractive index (RI) matching, which was followed by the next imaging and analysis procedure. PBS: phosphate-buffered saline; PBST: phosphate-buffered saline/0.2% Tween-20; PFA: paraformaldehyde; RI: refractive index.

https://dx.doi.org/10.21037/atm-21-2441

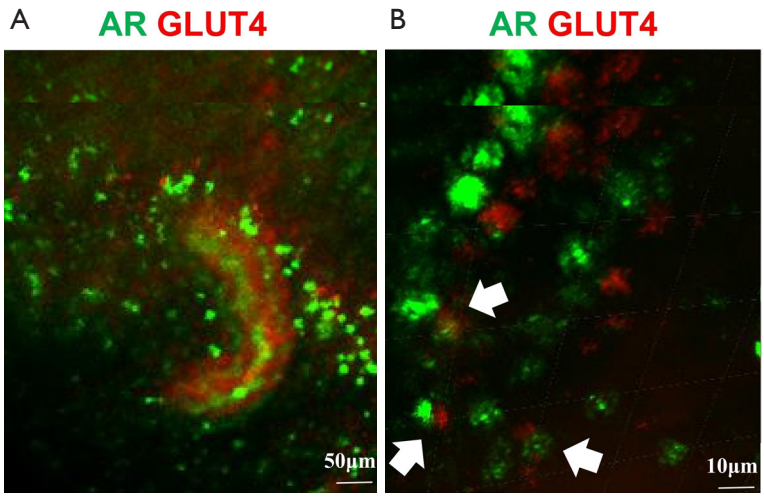

Figure S4 (A,B) Uteri from the control group were immunostained with anti-AR antibody (green) and anti-GLUT4 antibody (red). (B) The white arrows indicate the colocalization of AR with GLUT4 in the endometrium. AR: androgen receptor; GLUT4: glucose transportation protein 4.

https://dx.doi.org/10.21037/atm-21-2441

Table S1 Labeling reagents used in the protocol

Labeling reagent	Host	Vendor	Catalog	Dilution
Antiandrogen receptor	Rabbit	Abcam	Ab74272	1:100
Antiglucose transporter4	Mouse	Abcam	Ab35826	1:100
Goat antimouse IgG (H+L) cross-adsorbed secondary antibody, Alexa Fluor 488	Goat	Invitrogen	A-11001	1:200
Goat antimouse IgG (H+L) cross-adsorbed secondary antibody, Alexa Fluor 594	Goat	Invitrogen	A-11005	1:200
Goat antirabbit IgG (H+L) cross-adsorbed secondary antibody, Alexa Fluor 488	Goat	Invitrogen	A-11008	1:200
Goat antirabbit IgG (H+L) cross-adsorbed secondary antibody, Alexa Fluor 594	Goat	Invitrogen	A-11012	1:200
DAPI		Sigma	D9542	2 μg/ml

Table S2 Statistic methods used in the analysis

One-way ANOVA with Tukey multiple comparison post hoc test	One-way ANOVA (k samples)	Unpaired 2-tailed Student *t* test
Body weight from days 56, 6.3 and 70	Body weight on days 77 and 84	Body weight from days 0 to day 49
OGTT	E2	
FT, SHBG, LH, FSH, PRL, FINS	HOMA-IS	
HOMA-IR, HOMA-β	Myometrial volume	
Weight of ovary, weight of uterus	Gland volume	
Endometrial volume	Gland:myometrium volume ratio	
Endometrium-myometrium volume ratio	Fold-change over control of GLUT4 in the endometrium	
	Fold-change over control of GLUT4 in epithelial cells	
	Fold-change over control of GLUT4 in stromal cells	
	Fold-change over control of AR in the endometrium	
	Fold-change over control of AR in epithelial cells	
	Fold-change over control of AR in stromal cells	

ANOVA: analysis of variance; OGTT: oral glucose tolerance test; E2: estradiol; FT: free testosterone; SHBG: sex hormone-binding globulin; LH: luteinizing hormone; FISH: follicle-stimulating hormone; PRL: prolactin; FINS: serum fasting insulin; HOMA-IS: homeostatic model assessment insulin sensitivity; HOMA-IR: homeostatic model assessment insulin resistance; HOMA-β: homeostatic model assessment b-cell function; GLUT4: glucose transportation protein 4 antibody; AR: androgen receptor.

https://dx.doi.org/10.21037/atm-21-2441

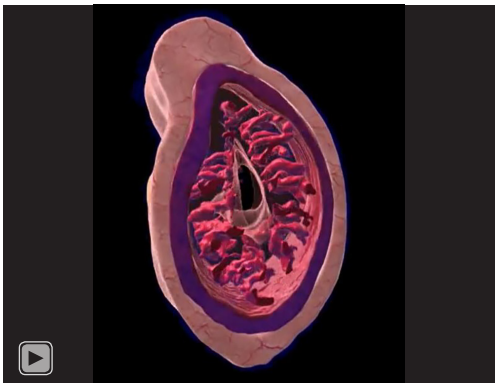

Video S1 Uteri were immunostained with DAPI (blue) and identified as endometrium, myometrium, and uterine glands.

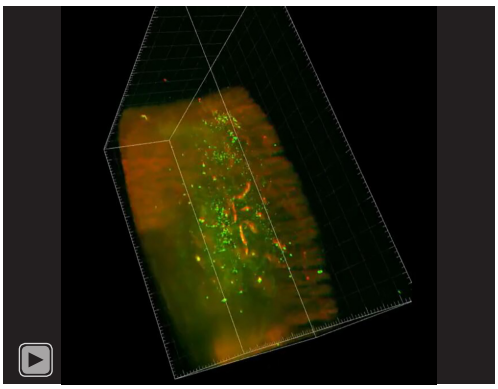

Video S2 Uteri were immunostained with anti-AR antibody (green) and anti-GLUT4 antibody (red).

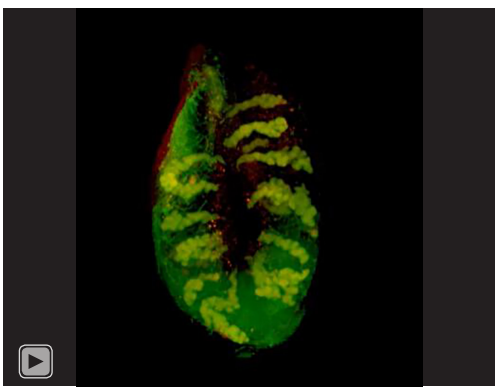

Video S3 Area-specific quantification of fluorescence signal intensity (green).

https://dx.doi.org/10.21037/atm-21-2441